International Journal of Heat and Mass Transfer 52 (2009) 2599–2606

Contents lists available at ScienceDirect

International Journal of Heat and Mass Transfer

journal homepage: www.elsevier.com/locate/ijhmt

# Numerical investigation of the heat and mass transfer in a vertical tube evaporator with the three-zone analysis

Il Seouk Park [a], Man Young Kim [b,*]

[a] Technical Research Laboratories, POSCO Co., Ltd., 1, Goedong-dong, Nam-Gu, Pohang, Gyeongbuk 790-785, Republic of Korea
[b] Department of Aerospace Engineering, Research Center of Industrial Technology, Chonbuk National University, 664-14 Duckjin-Dong, Duckjin-Gu, Jeonju, Chonbuk 561-756, Republic of Korea

ARTICLE INFO

*Article history:*
Received 25 April 2008
Received in revised form 17 December 2008
Available online 21 February 2009

*Keywords:*
Condensation
Evaporation
Film flow
Free surface
Vertical tube evaporator
Conjugate heat transfer

ABSTRACT

A numerical study for the flow, heat and mass transfer characteristics near the inflow region of the vertical evaporating tube with the films flowing down on both the inside and outside tube walls has been carried out. Condensation occurs along the outside wall and evaporation at the free surface of the inside film. The transport equations for momentum and energy are parabolized by the boundary-layer approximation and solved by using the marching technique. In this kind of numerical approach, the accurately predicting the early stage is really important because a small error at the previous step can produce the amplified big error at the next step. To accurately predict the flow at the inflow region of the vertical evaporating tube, the calculation domain of two film flow regions and tube wall is solved simultaneously. The interesting heat transfer characteristics revealed through this three-zone simulation, such as the evaporation delay and the temperature inflection at the very near inflow region are found and discussed along the discrepancy between the inner film inlet temperature and the saturation temperature. The case that the inner film comes in with the saturation temperature shows a good performance. The velocity and temperature fields as well as the amounts of the condensed and evaporated mass in both inner and outer films are predicted for the various conditions.



## 1. Introduction

In an evaporating tube bundle, evaporation and condensation occur simultaneously on the free surface of the each film flowing down on both sides of a vertical circular tube. A relatively colder fluid flows like a thin film along the inside wall, and therefore, the stagnant water steam outside of the tube becomes a condensation film, which flows down along the outside wall of the tube. This condensation film also induces evaporation on the free surface of the inside film of the tube. These vertical evaporating tube bundles are applied to a lot of engineering applications on which evaporation and condensation occur simultaneously, such as food industry, desalination and so on [1–4].

In a film flow heat transfer, the film thickness is the one of the most important parameters. The film has a different flow regime like laminar, laminar wavy, transition, and turbulent, along the film flow rate. Because the film thickness (or shape) depends on the flow regime, many studies for the relation between heat transfer and flow regime, and the turbulent transition have been conducted by many researchers such as Chun and Kim [5], and Seban and Faghri [6–8] for a couple of decades. Recently Krupiczka et al. [9] investigated the correlation between the Nusselt number and the boiling number in the range of high heat fluxes where nucleate boiling is developed. As a numerical study, although the applications and configurations (vertical or horizontal) were different, Stuhltrager et al. [10], Min and Choi [11] and Park and Choi [1] tried to solve the elliptic governing equation and track the film free surface to get a more accurate and realistic film thickness. Min and Choi [11] adopted an interface capturing method, the MAC [12] to get an accurate film shape including the surface tension effect for the LiBr–$H_2O$ absorption film on a horizontal tube. Park and Choi [1] used the moving grid technique [13,14] to find the three-dimensional shape of the condensation film flowing down along a vertical grooved tube. But their effectiveness and the accuracy when being extended to the high flow rate wavy regime is not affirmative for the efforts and costs for solving the elliptic equation set. The researchers returned to the parabolic governing equation simplified by the boundary-layer approximation. Feddaoui et al. [15] and Groff et al. [16] developed the boundary-layer based numerical method to cover both the liquid and gas sides, and be adequate to a wide range of the film and gas Reynolds number through testing a various turbulent models and comparing with the experimental results. As another research for the falling film heat transfer, in order to enhance the heat transfer, the adopting the grooved or fluted tube enlarging the heat transfer area has been tried by Park and Choi [1] and Jin et al. [3]. They found

* Corresponding author. Tel.: +82 63 270 2473; fax: +82 63 270 2472.
*E-mail address:* manykim@chonbuk.ac.kr (M.Y. Kim).

0017-9310/$ - see front matter © 2009 Elsevier Ltd. All rights reserved.
doi:10.1016/j.ijheatmasstransfer.2008.12.020

**Nomenclature**

| | |
|---|---|
| $u$ | velocity component in axial direction |
| $v$ | velocity component in radial direction |
| $r$ | radial coordinate component of position vector |
| $x$ | axial coordinate component of position vector |
| Fr | Froude number, $=U_i^{*2}/gD^*$ |
| Re | Reynolds number, $=U_i^*D^*/\nu$ |
| $T$ | temperature |
| Pr | Prandtl number, $\nu/\alpha$ |
| $g$ | gravitational acceleration, m/s$^2$ |
| $R_i$ | inner radius of tube |
| $R_o$ | outer radius of tube |
| $H_e$ | latent heat at the free surface of evaporating film, J/kg |
| $H_c$ | latent heat at the free surface of condensing film, J/kg |
| $q''$ | heat flux, W/m$^2$ |

*Greek symbols*

| | |
|---|---|
| $\alpha$ | thermal expansion coefficient, m$^2$/s |
| $\nu$ | kinematic viscosity, m$^2$/s |
| $\rho$ | density, kg/m$^3$ |
| $\Gamma$ | film flow rate |
| $\delta$ | film thickness |
| $\Delta x$ | increment of axial position at grid system |
| $\Delta r$ | increment of radial position at grid system |

*Subscripts*

| | |
|---|---|
| $i$ | inlet of inner film flow |
| $e$ | equilibrium (or saturated) state inside of tube |
| $o$ | outside of tube |
| $I$ | inner evaporating film zone |
| $II$ | solid tube body zone |
| $III$ | outer condensing film zone |
| $s$ | free surface |
| $p$ | previous axial position step at marching calculation |
| $old$ | the value which has been obtained at previous iteration step in an solving procedure |
| $new$ | the value newly obtained at present iteration step in an solving procedure |

*Superscript*

| | |
|---|---|
| $*$ | dimensional variable |

that the grooved or fluted tube showed an enhanced heat transfer by 5–10 times over a plain tube.

All these works, however, considered only an evaporating or condensing film existing at only one side of the tube. As an advanced approach, Wassenaar and Westra [17] considered three zones, i.e., plate wall, and cooling water and absorptive film on both sides of the tube. They developed a basic approach to solve a conjugated heat transfer problem with the mass and energy balance concept. However, they did not solve the complete form of the conservative equations, but rather, just used a lumped model in the tube radial direction. Therefore, the detailed developing process of the film could not be presented along the flow direction and the film region was still limited at one side of the tube.

In the boundary-layer method, the accurately calculating the initial stage is very important to understand the physics behind in the workings of a vertical tube evaporator because the wrong predicted flow variables at the previous step may cause the more wrong values at the next step. So it is highly necessary to solve simultaneously the heat and mass transfer phenomena in both the inner and outer films including the heat conduction of the tube wall, near the inlet zone.

In this work, the heat and mass transfer phenomena of two thin films and a conducting axisymmetric tube wall are analyzed simultaneously near the inlet region with the developed coupling technique for three different regions and their two interfaces. Since the calculation domain is limited on the very near entrance region ($x$ = 0.1–1 D), the evaporating film flowing in along the tube inside wall remains at a laminar no-wavy flow. The flow is described by the axisymmetric laminar boundary-layer equations, in which the diffusive terms for the primary flow direction are eliminated from the original elliptic-type conservative equations. The change of the film flow rate due to the evaporation and condensation are considered and the resulting film thickness changes are also predicted in the calculating procedure. The velocity and temperature fields, the amounts of the condensed and evaporated mass as well as the peculiar heat transfer characteristics near the inlet region are investigated for various inlet conditions.

In the following, after introducing a mathematical formulation for describing the flow, heat and mass transfer in a vertical tube evaporator, numerical results performed by changing such various parameters as inner pressure and film flow rate are presented. Finally, some concluding remarks are given.

## 2. Mathematical formulations

For the flow analysis of the inner and outer films in a vertical tube evaporator, it is assumed that (1) the pure water comes into the tube very calmly without turbulence (2) the properties of the fluid are constant in an operating range, (3) the interfacial shear forces at the film free surfaces are negligible because the surrounding steam vapors are stagnant and viscosities are much smaller than the liquid films', and (4) the saturated state is maintained at the free surface of the outer condensation film. Finally, (5) the boundary-layer approximation is adopted for the governing equations of the flow and heat transfer because the films are very thin and the flow has a distinct main flow direction.

### 2.1. Governing equations

The films flowing down along the tube inside and outside walls as shown in Fig. 1 can be described by the following nondimensional governing equations parabolized by a boundary-layer approximation, which was used by Feddaoui et al. [15] and Groff et al. [16], i.e.,

$$\frac{\partial(ru)}{\partial x}+\frac{\partial(rv)}{\partial r}=0 \tag{1}$$

$$u\frac{\partial u}{\partial x}+v\frac{\partial u}{\partial r}=\frac{1}{\mathrm{Fr}}+\frac{1}{\mathrm{Re}}\frac{1}{r}\frac{\partial}{\partial r}\left(r\frac{\partial u}{\partial r}\right) \tag{2}$$

$$u\frac{\partial T}{\partial x}+v\frac{\partial T}{\partial r}=\frac{1}{\mathrm{Re}\,\mathrm{Pr}}\frac{1}{r}\frac{\partial}{\partial r}\left(r\frac{\partial T}{\partial r}\right) \tag{3}$$

Here, $u=u^*/U_i^*$ and $v=v^*/U_i^*$ are the dimensionless velocity components of the dimensionless coordinates $x=x^*/D^*$ and $r=r^*/D^*$ directions, respectively. $T=(T^*-T_e^*)/(T_o^*-T_e^*)$ is the dimensionless temperature. Here, $U_i^*$ and $D^*$ are the mean velocity at the inlet of region I (the inner film zone) and the tube diameter, respectively. Also, $T_e^*$ and $T_o^*$ are saturation temperature for the

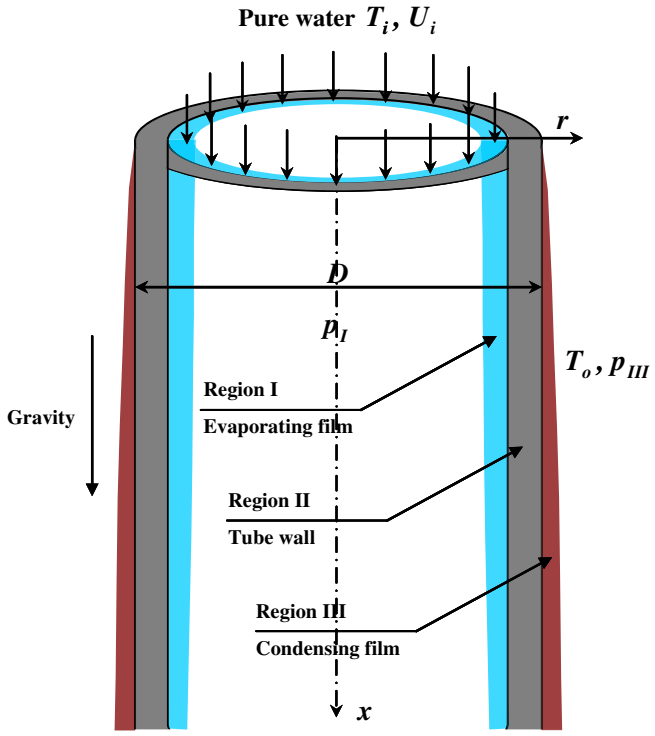


**Fig. 1.** Schematic view of the vertical tube evaporator with inner evaporation and outer condensation films.

steam pressure inside the tube and the temperature of steam vapor outside the tube, respectively. The nondimensional groups are defined as followings.

$$x=\frac{x^*}{D^*},\quad r=\frac{r^*}{D^*},\quad u=\frac{u^*}{U_i^*},\quad v=\frac{v^*}{U_i^*},\quad T=\frac{T^*-T_e^*}{T_o^*-T_e^*} \tag{4a}$$

$$\mathrm{Re}=\frac{U_i^*D^*}{\nu},\quad \mathrm{Fr}=\frac{U_i^{*2}}{gD^*},\quad \mathrm{Pr}=\frac{\nu}{\alpha} \tag{4b}$$

where, Fr, Re, and Pr indicate the Froude, Reynolds, and Prandtl numbers, respectively. $\nu$ is the kinematic viscosity, $g$ the gravitational acceleration, and $\alpha$ the thermal expansion coefficient. It is noted that $T_o^*$ is same as the temperature at the free surface of the outer film because it is assumed that the outer film is in direct contact with the saturated steam vapor without any thermal boundary-layer. If the water is flowing in the tube with the saturation temperature, $T_e^*$, the inflow water would immediately start to evaporate due to the heating by the steam outside the tube. If the water flows in with a lower temperature than $T_e^*$, the film will start to evaporate after the free surface temperature reaches $T_e^*$ along the tube axial direction. If the temperature of the entered water is higher than $T_e^*$, a kind of flashing phenomena is expected because the water will suddenly contact the low pressure steam while entering. In this study, these flash evaporating cases are excluded. The reference velocity, $U_i^*$ is defined as $\Gamma_I^*/(\rho_l D^* 2)$, where, $\Gamma_I^*$ and $\rho_l$ are the inlet mass flow rate and density of the inner film, respectively.

### 2.2. Boundary conditions

In order to analyze the heat and mass transfer for the tube wall and the two film flow regions which are separated by the tube, the following boundary conditions at the free surfaces and the flow inlets of the inner and outer film are adopted here, i.e.,

- at the free surface of inner film ($r = R_i - \delta_I$):

$$\frac{\partial u}{\partial r}=0 \tag{5a}$$

$$\frac{\partial T}{\partial r}=0 \text{ (for sensible heating zone, see Fig. 2)} \tag{5b}$$

$$T=0 \text{ (for evaporating zone, see Fig. 2)} \tag{5c}$$

- at the free surface of outer film ($r = R_o - \delta_{III}$):

$$\frac{\partial u}{\partial r}=0,\quad T=1 \tag{6}$$

- at the inlet of inner film ($x = 0$):

$$u=\frac{R_1\mathrm{Re}}{2(R_i+\delta_i)\mathrm{Fr}}[(R_i-r)^2+2\delta_i(R_i-r)] \tag{7}$$

- at the inlet of outer film $x = 0$:

$$u=0,\quad v=0,\quad T=1 \tag{8}$$

where $R_i$ and $R_o$ are the dimensionless inside and outside radii of the tube, while $\delta_I$ and $\delta_{III}$ the dimensionless film thicknesses of the inner and outer film, respectively. To consider the thermally developing progress for the case that the inner film flows in with a lower temperature than the saturation temperature, $T_e^*$, Eq. (5b) is used for the inner film free surface boundary condition until the free surface temperature of the inner film reaches the saturation temperature, $T_e^*$, like Fig. 2, as a sensible heating zone. The velocity profile in Eq. (7) is a quadratic expression which satisfies the no-shear condition at the free surface, and the no-slip condition and the following Eq. (9) at the wall:

$$-\frac{\mathrm{Re}}{\mathrm{Fr}}=\frac{1}{R_i}\frac{\partial}{\partial r}\left(R_i\frac{\partial u}{\partial r}\right) \tag{9}$$

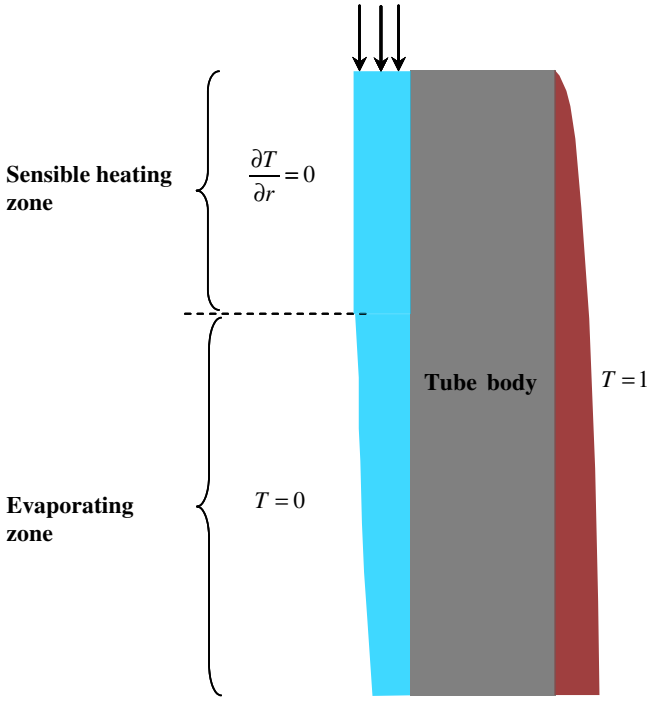


**Fig. 2.** Thermal boundary conditions at the free surfaces.

The temperature profile at the inlet of the inner film is obtained from one-dimensional analysis for the radial direction with the boundary condition of Eq. (5) at the free surface of the inner film and constant temperature, $T_o^*$ at the outer wall of the tube.

To compensate the film flow rates that are decreased by evaporation and increased by condensation, the following additional relations are adopted together with the above four boundary conditions, i.e.,

$$\Gamma_I^* = \Gamma_{I,p}^* - \frac{q''_{I,s}}{H_e} 2\pi(R_i^* - \delta_I^*)\Delta x^* \tag{10a}$$

$$\Gamma_{III}^* = \Gamma_{III,p}^* + \frac{q''_{III,s}}{H_c} 2\pi(R_o^* + \delta_{III}^*)\Delta x^* \tag{10b}$$

where $H_e$ and $H_c$ are the latent heat of evaporation and condensation per unit mass, respectively, while $q''_{I,s}$ and $q''_{III,s}$ are the heat fluxes at the free surfaces of the inner and outer film, respectively. It is noted that the analysis of the evaporating tube considered in this study is related to the conjugate heat transfer with three different regions and their two interfaces. To solve these situations the interfacial boundary conditions between the tube wall and films on both sides are needed at the inner and outer walls of the tube. These boundary conditions are explained in the next section.

### 2.3. Numerical analysis

To solve the governing equations for mass, momentum and energy with the above boundary conditions, it is necessary to discretize the equations with a numerical method. In this study, marching technique which was used by Feddaoui et al. [15] and Groff et al. [16] is adopted to solve the flow fields one-dimensionally in radial direction at the present $x$-step by using the results of the previous $x$-step. The $x$-derivative terms are discretized with 1st order backward differencing scheme and the $r$-derivative terms are discretized by 2nd order central differencing scheme as shown in Fig. 3. The 500 by 100 meshes in $x$- and $r$-directions are used for each film zone. The matrix of the discretized algebraic equation is solved with the tri-diagonal matrix algorithm (TDMA).

To track the film free surfaces whose positions (or film thicknesses) change along the $x$-direction due to evaporation and condensation, firstly mass, momentum and energy equations are solved with the film thicknesses of the previous $x$-step, thereby, the film flow rates increased or decreased due to condensation or evaporation are predicted by using the heat fluxes at the free surfaces like Eq. (10). Next, the new film thicknesses which satisfy the film flow rates updated from the previously calculated results, are guessed through the following relation:

$$\Gamma^* = \frac{\delta_{new}^*}{\delta_{old}^*} \int_0^{\delta_{old}^*} u_{old}^* dr^* \tag{11}$$

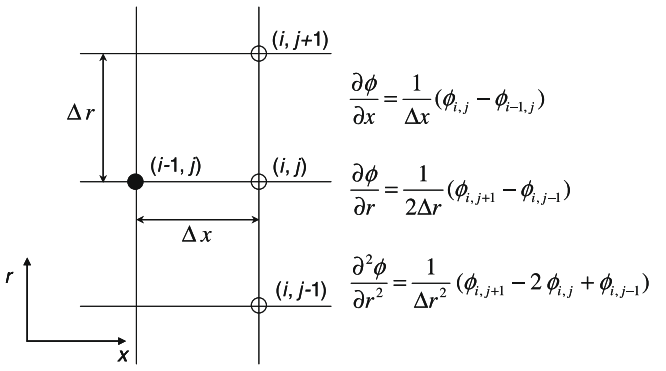


**Fig. 3.** Presentation of the node points and partial derivatives used in the differencing scheme.

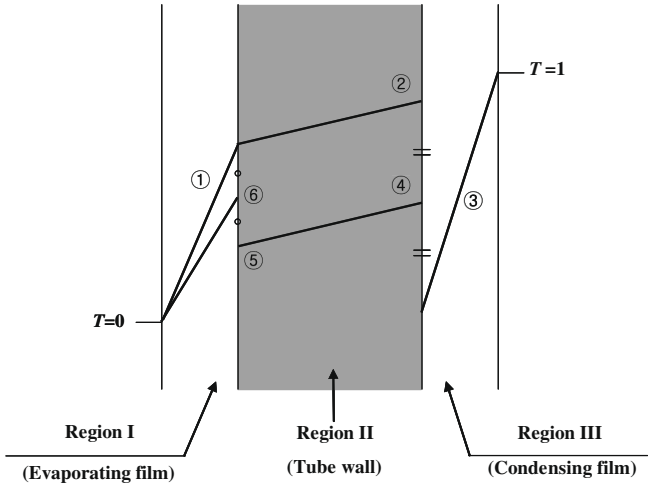


**Fig. 4.** Schematic of the solution procedure representing the three-zone analysis simultaneously including the inner evaporating, central conducting tube wall, and outer condensing films.

Then, the governing equations are reanalyzed with the newly updated film shape (i.e., thickness) through the iterative procedure of solving and updating. The film thickness is considered to converge if it does not change further within its changing rate of $(\delta_{new}^* - \delta_{old}^*)/\delta_{old}^* < 10^{-4}$.

The solution procedure developed for three-zone coupling is schematically shown in Fig. 4 and is summarized as follows.

*Step 1.* Solve the temperature field of region I by using the assumed temperature (usually the value of the previous $x$-step) at the inner wall of the tube.
*Step 2.* Solve the energy equation in region II (the solid tube body) using the temperature and heat flux at the inner wall obtained from the newest analysis for region I and then obtain the heat flux at the outer wall of the tube.
*Step 3.* Solve the temperature field of region III (the outer film zone) using the heat flux at the outer wall obtained from Step 2 and the saturation temperature at the free surface of the outer film as the boundary conditions.
*Step 4.* Update the new outer wall temperature with the arithmetic mean of the outer wall temperatures of Steps 2 and 3.
*Step 5.* Solve again the temperature field in region II using the outer wall heat flux used in Step 3 and the outer wall temperature newly updated from the Step 4 and then obtain the new inner wall temperature.
*Step 6.* Recalculate the temperature field of region I by setting the inner wall temperature with the arithmetic mean of the inner wall temperature used in Step 1 and the value newly obtained from Step 5.
*Step 7.* Repeat the Steps 2–6 until the temperature changes at the inner and outer walls remain below $10^{-4}$.

## 3. Results and discussion

To validate the present numerical approach which tracks the free surface position with the boundary-layer type equation set, for the film coming in with the wrong film thickness and velocity profile along a tube outside wall, the developing progress to the right value is investigated. The film flow along a vertical tube wall has an exact solution. The film has the constant film thickness and zero radial velocity like Eq. (12) when the flow is fully developed and remains laminar as discussed by Nusselt [18].

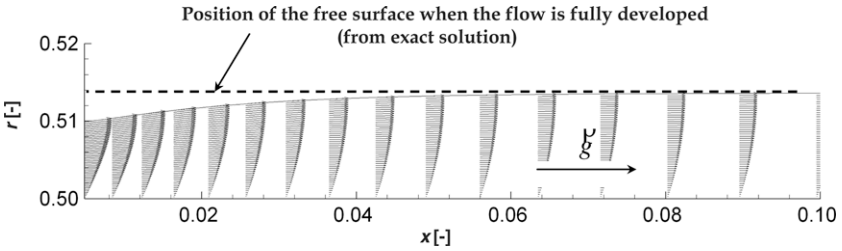


**Fig. 5.** Validation of the free surface tracking.

$$u^* = -\frac{g}{4\nu}(r^{*2} - R_o^2) + \frac{g}{2\nu}(R_o + \delta^*)^2 \ln\frac{r^*}{R_o} \tag{12a}$$

$$v^* = 0 \tag{12b}$$

When the film starts to flow into the tube with an initial arbitrary film thickness, as shown in Fig. 5, the film develops to the thickness which is obtained from the exact solution of Eq. (12), at a same film flow rate. Here, it is noted that the film flow is fully developed before it reaches $0.1 \times D^*$, and the predicted film thickness is quite same as that from the exact solution when the flow is fully developed.

To check up how the developed code simulates that the film thickness varies by the evaporation and condensation, the flow fields are investigated for a very small inner film flow rate, 0.0001 kg/s, which will not be adopted in a real engineering problem, in Fig. 6. The inner film becomes thin due to evaporation as the film flows down. In contrast, the outer film becomes thick because of the condensation. In Fig. 7, in order to quantitatively validate the code, the developing progresses of the condensation film thickness are compared with the classic Nusselt's solution [18]. The test was conducted for the condensation on the inclined plate. The wall temperature is 65 °C, the saturation temperature, 70 °C. The results by Nusselt and present code show a quite good agreement.

The effect of inner pressure on the initial development process of film flow and heat transfer, especially, in the extremely short length zone with 10% tube diameter is depicted in Fig. 8 (OD is 25 mm, so the length of the calculation domain is 2.5 mm). Here, inner film flow rate is set to 0.05 kg/s, inner pressure has three different value of 58 kPa, 65 kPa, and 70 kPa, and for all cases the films are coming in with 85 °C, where the temperature, 85 °C is analogous to the saturation temperature for the inner pressure, 58 kPa. In the figure, the change of the inner film thickness does not be distinguished because of the large inner film flow rate and a very short calculation domain. Also, note that the evaporation of the inner film is delayed more as the inner pressure becomes greater than the saturation pressure. For the case of 58 kPa, the isotherms of the inner film are seen to be almost parallel to the free surface, while for the cases of 65 and 70 kPa the isotherms cross perpendicular to the free surface in the short regions near the inlet. This means the heat from the outer film or steam is used only for heating the inner film not evaporating in this small area (sensible heating zone).

Figs. 9 and 10 show the effect of inner pressure on qualitative change of flow rates of the inner and outer films, respectively, for the case of $\Gamma_I^* = 0.05$ kg/s. Here, nondimensional flow rates normalized by the inner film flow rate at the inlet are presented. If the flow rate decreases to −1, the inner film becomes completely dried out. The inner and outer films have different thermal

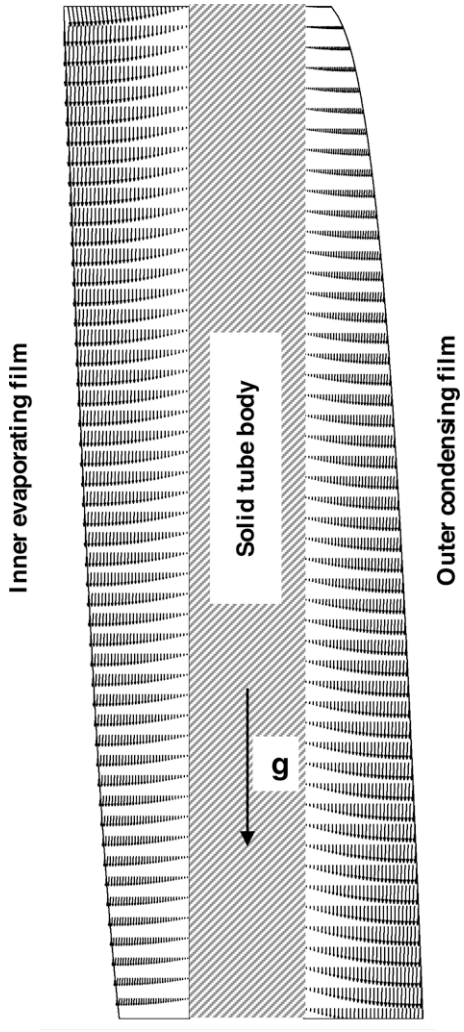


**Fig. 6.** Velocity vectors in the inner and outer films when $\Gamma_I^* = 0.0001$ kg/s. The solid lines in both films represent the outer free surfaces of each film.

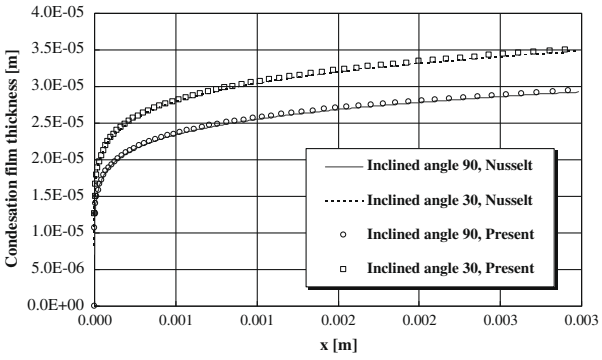


**Fig. 7.** Comparison of the film thickness developments by Nusselt analysis and present code for the condensation film on an inclined plate.

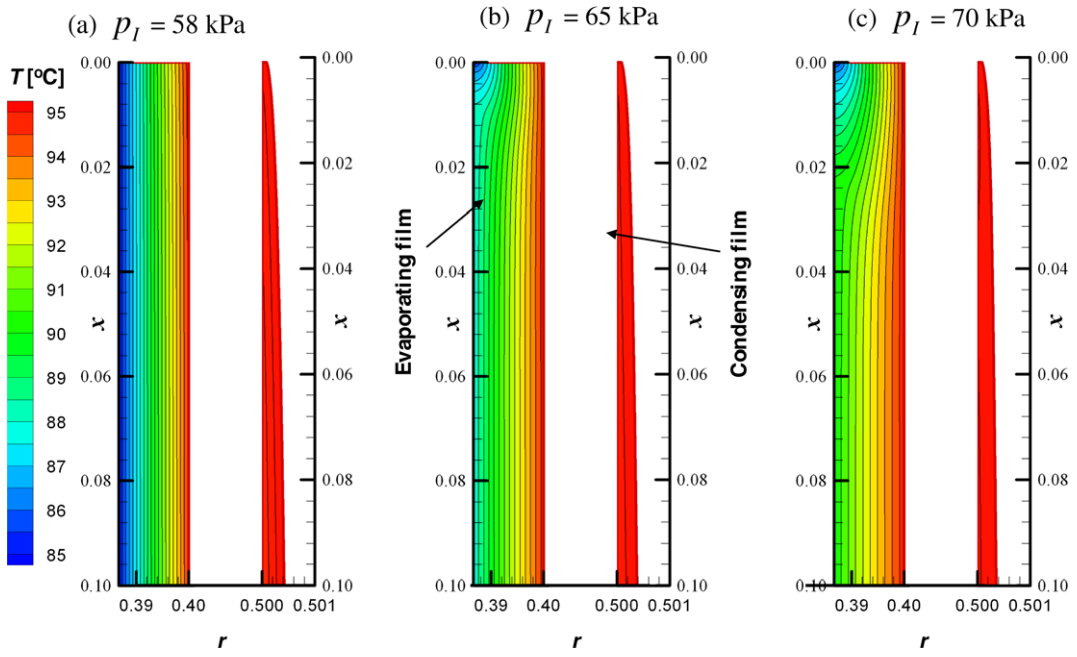


**Fig. 8.** Isotherms of the inner and outer film zones when $\Gamma_I^* = 0.05$ kg/s: (a) $p_I$ = 58 kPa, (b) $p_I$ = 65 kPa, and (c) $p_I$ = 70 kPa.

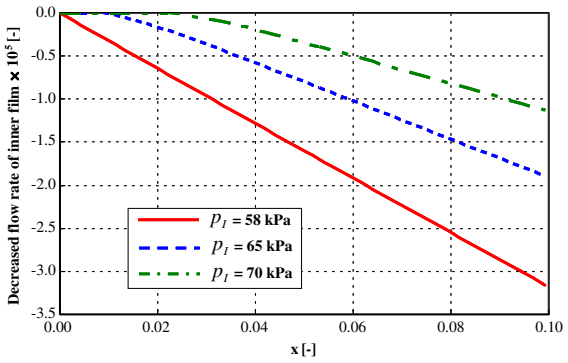


**Fig. 9.** Decreased flow rate of the inner film due to evaporation for various inner pressure conditions when $\Gamma_I^* = 0.05$ kg/s.

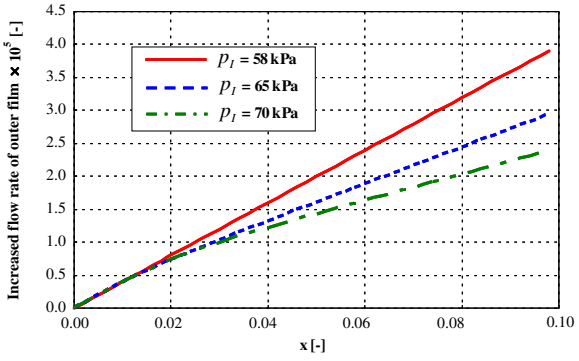


**Fig. 10.** Increased flow rate of the outer film due to condensation for various inner pressure conditions when $\Gamma_I^* = 0.05$ kg/s.

behavior because of different phenomena occurring in inner and outer films, i.e., evaporation and condensation, respectively. If the inner pressure is 58 kPa, the inner film coming to the tube inside starts to evaporate immediately because the inlet temperature of the inner film, 85 °C, is exactly same as the saturation temperature of the inner pressure, 58 kPa, as shown in Fig. 9. When the inner pressure increases to 65 kPa, however, the film evaporates after the inner film is heated by the steam outside the tube and its free surface temperature reaches the increased saturation temperature of 88 °C. Finally, when the inner pressure becomes 70 kPa, because saturation temperature rises to 90 °C, the inner film starts to evaporate at more downstream than the lower pressure cases. Fig. 10 illustrates flow rate of the outer film, where condensation occurs. For the inner pressure of 58 kPa, much more steam is condensed at the inlet region because the inner film evaporates immediately at the inlet and the evaporation heat begins to be discharged at much more early position than the cases of 65 and 70 kPa, where the evaporation does not occur at this very near inlet region. Also, it can be found that less steam condenses as the inner pressure increases because of delayed evaporation in the inner film. Here, it is noted that the increasing rates of outer film flow rate are different each other beyond $x$ = 0.02. This is because the energy potential to transport the heat and mass accompanying phase changes becomes smaller as the inner pressure increases.

Fig. 11 shows variation of the mean and wall temperature of the inner evaporative film along the axial direction. For the cases of the inner pressure 65 and 70 kPa, which are not a saturation state at the inlet region, the mean temperatures show a sharp increase at the very near inlet region because the inner film is heated until the free surface temperatures of the film becomes the saturation temperature. This retards the condensing performance of the outer film, which condensates the outside steam. Therefore, the condensed amounts are smaller than the case of the inner pressure 58 kPa as shown in Fig. 10. Also because the heat from the outside steam is only used for the temperature increase of the inner film and not used for the evaporation, there is no heat discharge to the tube inside by the evaporation, therefore the condensation of the outer film is retarded. The wall temperature of the tube inside is also shown in Fig. 11. For the case of 58 kPa temperature continuously decreases because of the cooling effect of the inner film. However, as the inner pressure increases to 65 and 70 kPa, an inflection point appears near the inlet where evaporation occurs. The phenomenon is also found in the outer film as shown in

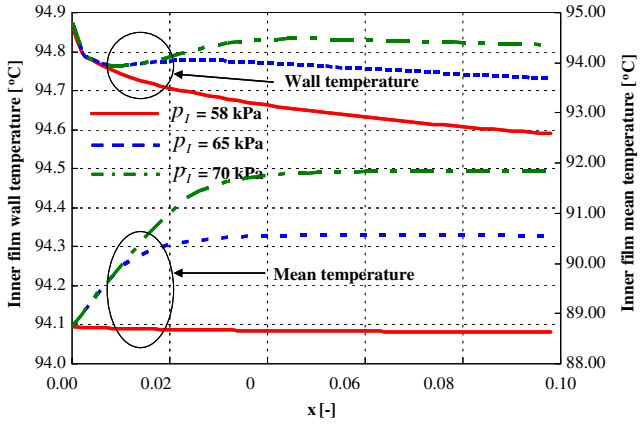


**Fig. 11.** Variation of the mean and wall temperatures of the inner film along the tube axis direction for various inner pressure conditions when $\Gamma_I^* = 0.05$ kg/s.

Fig. 12. This is because the heat does not be discharged locally on the inner film free surface because of the evaporation delay at the inlet region even though the condensation heat of the outer film is provided into the inner film. For the case of very small inner film flow rate of 0.0001 kg/s, the predictions of the decreased and increased flow rates of inner and outer films are given in $1 \times D^*$ length zone as shown in Figs. 13 and 14. Here, it is noted that the dimensionless increased and decreased flow rates are much larger than those of the cases of large flow rate of 0.05 kg/s, given above. This is due to the fact that heat transfer occurs very actively for small flow rate because of the very thin film thickness. Also, it can be found that the decreased flow rate of the inner film nearly reaches to $-1$ at the tube length $D^*$ for the case of the inner pressure of 58 kPa, and the increased flow rate of the outer film also nearly reaches to 1. This means that most of the entered inner film is vaporized at the $1 \times D^*$ axial position. Note that the inner film looks like to start to vaporize immediately at the inlet region without any evaporation delay regardless of the inner pressure. This is because the heat is spread very rapidly since the film is initially very thin. It is observed that the temperature is also developed fast and the free surface temperature of the inner film immediately reaches the saturation temperature. Even though the evaporations start from nearly same axial position, the evaporated and condensed amounts are quite different each other depending on the inner pressure. The case of the inner pressure closer to the saturation pressure evaporates and condenses much more vapor. This is

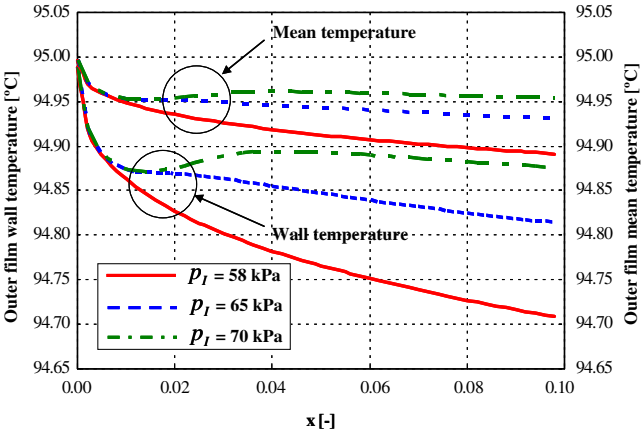


**Fig. 12.** Variation of the mean and wall temperatures of the outer film along the tube axis direction for various inner pressure conditions when $\Gamma_I^* = 0.05$ kg/s.

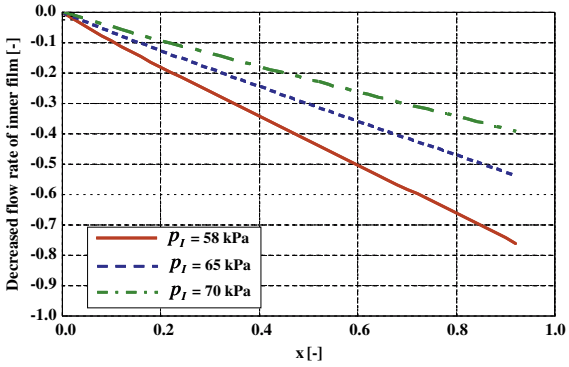


**Fig. 13.** Decreased flow rate of the inner film due to evaporation for various inner pressure conditions when $\Gamma_I^* = 0.0001$ kg/s.

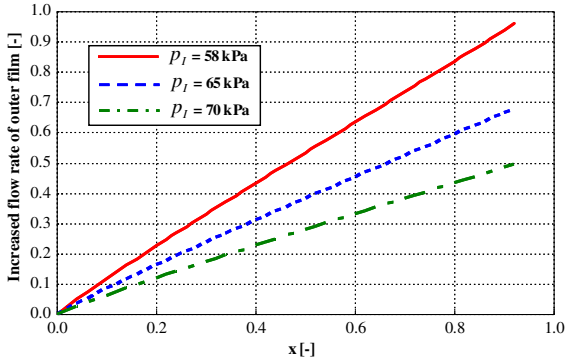


**Fig. 14.** Increased flow rate of the outer film due to condensation for various inner pressure conditions when $\Gamma_I^* = 0.0001$ kg/s.

because the temperature of the inner film is dependent on the inner pressure. Therefore a lower inner pressure ensures a larger temperature difference between the inner and outer films.

## 4. Conclusions

In this work, the influence of the discrepancy between the feed water temperature and the tube inside saturation temperature has been investigated. To understand the heat and mass transfer phenomena induced by this discrepancy, the detailed analysis for the very short inlet region has been conducted. The three-zone coupling technique and free surface tracking method for the boundary-layer based approach has been developed. Through the present detailed analysis for the near inlet region, the followings are revealed: The evaporation delay and the film temperature inflection appear at the very near inlet region when the inner film comes into the tube with the lower temperature than the saturation temperature. This evaporation delay and the temperature inflection deteriorate the evaporating and condensing performance. The making-up the feed temperature of the inner film as a saturation temperature is helpful for effectively using the heat transfer area and enhancing the heat transfer efficiency.

## References

[1] I.S. Park, D.H. Choi, Heat- and mass-transfer analysis for the condensing film flow along a vertical grooved tube, Int. J. Heat Mass Transfer 44 (2001) 4277–4285.
[2] A.H. Khan, Desalination Processes and Multistage Flash Distillation Practice, Elsevier, Berlin, 1986.
[3] W.X. Jin, S.C. Low, Terence Quek, Preliminary experimental study of falling film heat transfer on a vertical doubly fluted plate, Desalination 152 (2002) 201–206.

[4] J.S. Prost, M.T. Gonzalez, M.J. Urbicain, Determination and correlation of heat transfer coefficients in a falling film evaporator, J. Food Eng. 73 (2006) 320–326.
[5] Moon-Hyun Chun, Kyun-Tae Kim, Assessment of the new and existing correlations for laminar and turbulent film condensations on a vertical surface, Int. Commun. Heat Mass Transfer 17 (1990) 431–441.
[6] R.A. Seban, A. Faghri, Film condensation in a vertical tube with a closed top, Int. J. Heat Mass Transfer 27 (1984) 9447–9948.
[7] R.A. Faghri, A. Seban, Heat transfer in wavy liquid films, Int. J. Heat Mass Transfer 28 (2) (1985) 506–508.
[8] A. Faghri, R.A. Seban, Heat and mass transfer to a turbulent liquid film, Int. J. Heat Mass Transfer 31 (4) (1988) 891–894.
[9] Roman Krupiczka, Adam Rotkegel, Zenon Ziobrowski, Heat transfer to evaporating liquid films within a vertical tube, Chem. Eng. Process. 41 (2002) 23–28.
[10] E. Stuhltrager, N. Yutaka, M. Akio, U. Haruo, Flow dynamics and heat transfer of a condensate film on a vertical wall – I. Numerical analysis and flow dynamics, Int. J. Heat Mass Transfer 36 (6) (1991) 1677–1686.
[11] J.K. Min, D.H. Choi, Analysis of the absorption process on a horizontal tube using Navier–Stokes equations with surface-tension effects, Int. J. Heat Mass Transfer 42 (1999) 4567–4578.
[12] F.H. Harlow, J.E. Welch, Numerical calculation of time-dependent viscous incompressible flow of fluid with free surface, Phys. Fluids 8 (1965) 2182–2189.
[13] S. Muzaferija, M. Peric, Computation of free-surface flows using the finite-volume method and moving grids, Numer. Heat Transfer B 32 (1997) 369–384.
[14] J.L. The, G.D. Raithby, G.D. Stubley, Surface-adaptive finite-volume method for solving free surface flows, Numer. Heat Transfer B 26 (1994) 267–380.
[15] M. Feddaoui, A. Mir, E. Belahmidi, Cocurrent turbulent mixed convection heat and mass transfer in falling film of water inside a vertical heated tube, Int. J. Heat Mass Transfer 46 (2003) 3497–3509.
[16] M.K. Groff, S.J. Ormiston, H.M. Soliman, Numerical solution of film condensation from turbulent flow of vapor–gas mixtures in vertical tubes, Int. J. Heat Mass Transfer 50 (2007) 3899–3912.
[17] R.H. Wassenaar, J.J.W. Westra, Dynamic model of a film absorber with coupled heat and mass transfer, Int. J. Heat Mass Transfer 35 (1) (1992) 87–99.
[18] W. Nusselt, Die Oberflachen Kondensation des Wasserdampes, Zeitsehrit des Vereines Deutscher Ingenieure 60 (1916) 541–546. 569–575.